Available online at www.sciencedirect.com
SCIENCE DIRECT
Earth and Planetary Science Letters 244 (2006) 97 – 112
EPSL
www.elsevier.com/locate/epsl

Melt extraction in the Earth's mantle: Constraints from U–Th–Pa–Ra studies in oceanic basalts

Andreas Stracke [a,*], Bernard Bourdon [b,1], Dan McKenzie [c]

[a] Max-Planck-Institut für Chemie, Postfach 3060, 55020 Mainz, Germany
[b] Laboratoire de Géochimie et Cosmochimie IPGP-CNRS UMR7579, 4 Place Jussieu, 75252 Paris Cedex 05, France
[c] Bullard Laboratories, Department of Earth Sciences, Cambridge University, Madingley Road, Cambridge, CB3 0EZ, UK

Received 10 August 2005; received in revised form 17 January 2006; accepted 23 January 2006
Available online 9 March 2006
Editor: K. Farley

Abstract

U-series studies in oceanic basalts are critical for understanding melting and melt extraction in the Earth's mantle. The combined results of a detailed geochemical study of melting and melt extraction at Theistareykir, northern Iceland, provide a strong case for melt extraction via channeled melt flow at an active spreading ridge. It has often been argued, however, that widely used melting and melt extraction models, which simulate channeled melt extraction (i.e. fractional and/or dynamic melting), can only partially explain the global U-series systematics in oceanic basalts. As a consequence, more complicated models have been invoked, which suggest different styles of melt extraction at different depths/pressures in the mantle, so-called "two-porosity models". Alternatively, diffusion-controlled mechanisms have been proposed. Here we show that U–Th–Pa–Ra systematics in oceanic basalts can indeed be explained by models where melt transport occurs without chemical equilibrium between melt and solid when variations in all three critical melting parameters (residual porosity, upwelling rate of the solid mantle and melt velocity) are taken into account. Melting at ridges requires systematic variation of at least two critical melting parameters, most likely upwelling and melt extraction rate. Melts generated with increasing lateral distance to the ridge axis are generated with slower upwelling rates and are extracted with lower velocities than melts created closer to the ridge axis. Melting at ocean islands, on the other hand, can successfully be explained by variations in upwelling rate only. Global U-series systematics in OIB originate from superimposed global variations in upwelling velocity due to different buoyancy fluxes and from local variation in upwelling velocity as a function of radial distance to the plume center. The model proposed here is consistent with other geochemical data for oceanic basalts and strongly supports melt extraction via high-porosity channels as a general means of melt extraction from the Earth's upper mantle.

Keywords: U-series; MORB; OIB; melt extraction; dynamic melting

1. Introduction

Despite numerous geophysical and geochemical studies, our knowledge about mantle melting and melt extraction remains limited. The fluid dynamical process of melt movement is theoretically described by two-

* Corresponding author. Fax: +49 6131 371051.
E-mail address: stracke@mpch-mainz.mpg.de (A. Stracke).
[1] Now at: Institut für Isotopengeologie und Mineralische Rohstoffe, Department of Earth Sciences, ETH-Zürich, CH-8092, Zürich, Switzerland.

0012-821X/$ - see front matter © 2006 Elsevier B.V. All rights reserved.
doi:10.1016/j.epsl.2006.01.057

phase flow [1,2]. These equations require melt to move in chemical equilibrium with the solid and support solitary waves in one, two, or three dimensions. Only three-dimensional solitary waves are stable [3–5], however, and there is, as of yet, no evidence for the existence of such waves in the melting regions in the Earth's upper mantle. Moreover, time scales of melt transport of about 1000 years or less are incompatible with solitary wave transport and require melt to move in channels with a minimum dimension of a few millimeters [6]. Such channels may be formed by chemical [7,8] or mechanical processes. Since direct observations of the physical process of melting and melt movement in the mantle are unavailable and geophysical studies lack the necessary resolution, geochemical and petrological tools appear, at this time, to be most promising for studying melting and melt extraction.

The comprehensive study of basaltic melt generation, melt movement and source composition at Theistareykir, northern Iceland [9–17], has shown that melting at Theistareykir occurs as a result of passive decompression melting at shallow depths (<about 80 km) with a possible component of active upwelling at greater depths [18,19]. Slater et al. [15] showed that mixing of instantaneous fractional melts reproduces the chemical composition of the melt inclusions and the erupted melts by incomplete mixing of instantaneous fractional melts from different depths of the melting region [11,12,15]. Erupted melts at Theistareykir, even those from a single flow, also preserve considerable compositional variability [11,15,16]. Decreasing compositional variability in melt inclusions with decreasing fosterite content in olivine phenocrysts indicate that mixing and crystallization occur concurrently at Moho depths or deeper [11]. Thus melts entering major sites of melt pooling and mixing (magma chambers?) must have preserved considerable compositional heterogeneity, indicating that melt mixing during transport from the source region to the surface is incomplete.

A detailed isotopic and geochemical investigation of the Theistarykir melts [16] showed that erupted melts also preserve considerable isotopic heterogeneity, indicating that the source region is composed of at least two isotopically heterogeneous components. Isotopic variation in the Theistareykir melts is well-correlated with major element and trace element variability [16]. Thus the erupted lavas represent variable mixtures of melts from different depths and regions with different isotopic compositions. The combined geochemical results from Theistareykir show that melts must be able to move to magma chambers with little interaction with the material through which they pass and retain correlations between different isotopes, trace elements and major elements right through to eruption as lavas on the surface. This behavior is most readily explained if melt transport occurs in a channeled network and not by porous flow.

Simple porous flow cannot produce extraction velocities greater than 2 m/yr [8]. The rates of melt transport therefore provide another important constraint on melt transport mechanisms (e.g. [6]). Maclennan et al. [10] argue that a peak in eruption rates occurred immediately after the end of the last glacial period with concurrent melt extraction velocities greater than 50 m/yr. Such high velocities cannot be generated by porous flow and require melt flow to be in channels or along fractures. Potential variations in either mantle upwelling rate and/or melt extraction velocities have also been discussed as a potential explanation for the variation in excess ^{230}Th in the Theistareykir lavas [17]. Taken together, the observations discussed above provide a strong case for channeled melt transport at Theistareykir.

Here, we use new U–Pa data from Theistareykir in combination with global U–Th–Pa–Ra data from MORB and OIB to put further constraints on melting and melt extraction mechanisms beneath Theistareykir, and mid-ocean ridges and ocean islands in general. In particular, we address the following questions: 1) Does the new Pa data complement the existing picture of melting and melt extraction at Theistareykir? 2) Can U–Th–Pa–Ra data in oceanic basalts in general be explained by melting models that simulate channeled melt flow (fractional or dynamic melting), or are more complicated models required? 3) What are the mechanisms and timescales of melt extraction beneath ridges and ocean islands?

2. Modeling U-series disequilibria with dynamic melting

The maximum melt extraction time is constrained by the half-life of the shortest-lived radioactive isotope out of isotopic equilibrium [20]. U-series data can therefore provide important model-independent order of magnitude constraints on the timescales of melt extraction. More precise absolute estimates of the critical melting parameters, upwelling rate of the solid mantle (W), melt extraction velocity (v), and residual porosity (ϕ), however, depend on model calculations. While the relative variations between these model-derived parameters are robust, the accuracy of absolute estimates relies on how well the applied model approximates the natural system.

The melting model used here has been described in detail in Stracke et al. [17] and is an incremental solution to dynamic melting [21,22] with pressure-dependent changes in source mineralogy and compositionally dependent variations of mineral-melt partition coefficients. ^{230}Th–^{231}Pa–^{226}Ra excesses are calculated based on the assumption of initial secular equilibrium (i.e. (^{230}Th/^{238}U)=(^{231}Pa/^{235}U)=(^{226}Ra/^{230}Th) source=1), and considering ingrowth of ^{230}Th–^{231}Pa–^{226}Ra in the residue, which is directly dependent on the upwelling velocity of the solid mantle, and decay of ^{230}Th–^{231}Pa–^{226}Ra as a function of melt extraction velocity. In contrast to previous analytical solutions to dynamic melting, which for simplicity assume zero melt extraction time or infinite melt extraction velocity (e.g. [22–24]), the numerical model used here offers the possibility to vary melt extraction rates and the preferred depth of melt pooling (i.e. melt travel distance to magma chambers). Similar to the original analytical solution [22], no interaction between the melt and residue takes places during melt extraction, and the residual porosity (ϕ) is constant. For dynamic melting, ^{230}Th–^{231}Pa–^{226}Ra excesses are dominated by the initial stages of melting, and are little affected by later stages of melting because U and Th are quantitatively removed from the residue after only a few percent of melting (<~2–5%). Variations in ^{230}Th–^{231}Pa–^{226}Ra excesses in MORB and OIB due to variable residual porosity therefore mainly reflect changes in initial porosity, whereas depth-dependent porosity variations play little role.

Using dynamic melting with finite melt transport velocity [17], ^{230}Th–^{231}Pa–^{226}Ra excesses are dependent on the melting rate, which is proportional to the upwelling velocity of the solid mantle (W), the melt ascent velocity (v) and the residual porosity (ϕ), in addition to the partition coefficient values. Because of the different half-lives of the daughter isotopes (^{230}Th ~75,000 years, ^{231}Pa ~32,500 years, and ^{226}Ra ~1600 years) each decay system responds differently to changes in W, v and ϕ. For simplicity, a constant set of partition coefficient values is used for the modeling in Sections 3 and 4 (Table 1). The influence of changing partition coefficient values will be discussed in detail in Section 5.

All three critical melting parameters (W, v, and ϕ) influence ^{230}Th, ^{231}Pa and ^{226}Ra excesses, although in different fashion, depending on the element considered and its respective half-life. Slow upwelling rates (W), fast melt extraction velocities (v) and low residual porosity (ϕ) all lead to large ^{230}Th excess (Fig. 1), but W has the largest influence on (^{230}Th/^{238}U) ratios. This also holds for the ^{235}U–^{231}Pa decay system, but because of the approximately two times shorter half-life of ^{231}Pa compared to ^{230}Th, the ^{235}U–^{231}Pa decay system provides better resolution at shorter timescales (about three to four times the half-life of ^{231}Pa, i.e. about 100,000 years) and is also more sensitive to variations in upwelling and melt extraction velocity than the ^{238}U–^{230}Th decay system (Fig. 1a,b). Owing to the slow mantle upwelling rates (W) beneath ridges and ocean islands (a few cm/year) and the short half-live of ^{226}Ra, ^{230}Th and ^{226}Ra maintain (or stay close to) secular equilibrium in the residual mantle during melting, and (^{230}Th/^{226}Ra) ratios are effectively dependent on v and ϕ only. Fast melt extraction velocities (v) and low residual porosity (ϕ) lead to large ^{226}Ra excess (Fig. 1c,d).

The critical melting parameters W, v, and ϕ can be varied independently of each other in the melting model applied here, and thus no a priori assumption about the relationship between W, v and ϕ is made. Dynamic melting with finite melt transport velocity [17] therefore allows derivation of an empirical relationship between W, v and ϕ from the constraints given by the ^{230}Th–^{231}Pa–^{226}Ra data in MORB and OIB. In contrast to previous dynamic melting models, mixing between melts generated from regions with different melting properties, which take variable times to reach the surface, is considered in the following discussion. It is

Table 1
Preferred U–Th partition coefficient values

	ol	opx	Low Ca cpx	High Ca cpx	gt	sp
U	0.00038	0.002	0.0113	0.0094	0.028	0
Th	0.00005	0.002	0.0057	0.0059	0.009	0
Pa	0	0.0000027	0	0	0.005	0
Ra	0.000001	0.00001	0.00005	0.00005	0	0
Modal composition	ol	opx	cpx		gt	sp
Garnet stability field	0.53	0.08	0.34		0.05	0
Spinel stability field	0.53	0.26	0.18		0	0.03

Sources of U and Th partition coefficient data [50,52,72]. Pa and Ra partition coefficients are estimated following the discussion in [45]. For further details of the modeling parameters see [17].

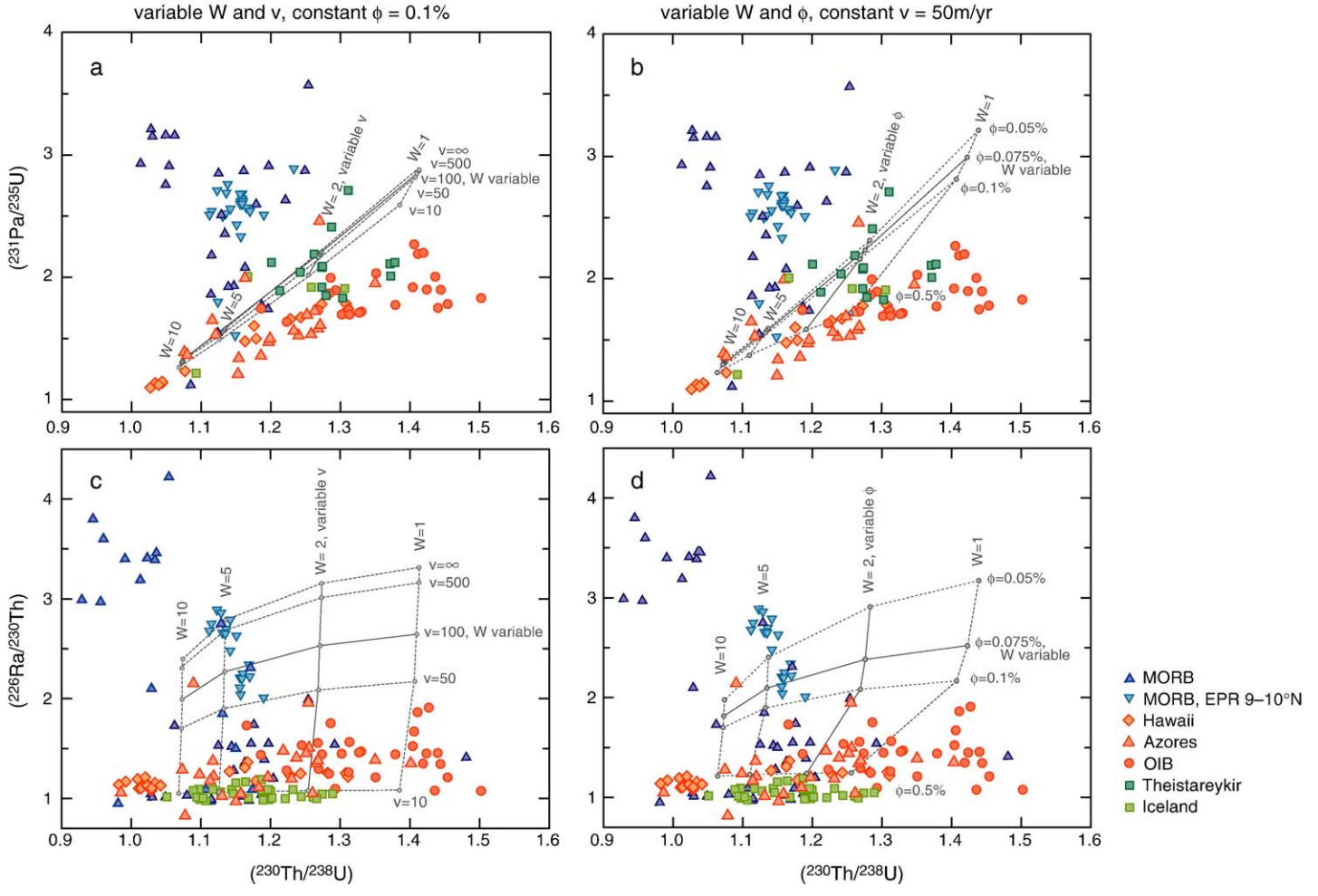

Fig. 1. Plot of (a) and (c) (^{231}Pa/^{235}U) versus (^{230}Th/^{238}U) and (b) and (d) (^{226}Ra/^{230}Th) versus (^{230}Th/^{238}U) in MORB and OIB. Grid shows calculated variations in (^{231}Pa/^{235}U) and (^{230}Th/^{238}U) and (^{226}Ra/^{230}Th) and (^{230}Th/^{238}U) as a function of upwelling rate (W [cm/yr]) and melt extraction velocity (v [m/yr]) in (a) and (c) and upwelling rate (W) and porosity (ϕ [%]) in (b) and (d). Calculations are done using the model described in detail in Stracke et al. [17] assuming a degree of melting of 10%, an initial depth of melting of 90 km and melt transport to the base of the lithosphere at 10 km. Mineral-melt partition coefficient values are given in Table 1. Note that (^{231}Pa/^{235}U), (^{226}Ra/^{230}Th) and (^{230}Th/^{238}U) ratios are not provided on all sample series, which accounts for differences in (a) and (b) and (c) and (d). Data sources are: MORB: [46,47,74–76]; EPR-MORB: [31,77]; Hawaii: [29–31,36,78]; Azores: [39,44]; OIB: [26,37,38,79]; Theistareykir: this study and [17]; Iceland: [43,78].

these relationships between residual porosity (ϕ) and solid and melt velocities (W and v) that are critical for understanding melting and melt extraction mechanisms in the oceanic upper mantle.

3. Melting and melt extraction beneath Theistareykir

Although Iceland is not a "normal" ridge setting, melting at Theistareykir occurs as a result of passive mantle upwelling at shallow depths (<about 80 km) with a possible component of active upwelling at greater depths (e.g. [18,19]) and is a reasonable proxy to melting beneath "normal" ridges. U–Th isotope systematics previously discussed by Stracke et al. [17] suggest that the excess ^{230}Th of the erupted melts could be influenced by different melt transport times. The ^{238}U–^{230}Th decay system (half-life of ^{230}Th ~75,000 years), however, lacks the necessary sensitivity to resolve small differences in upwelling and melt extraction velocities.

New U–Pa data are presented in Table 2 and allow additional constraints on melt extraction (half-life of ^{231}Pa ~32,500 years) at Theistareykir. The age of the Theistareykir rocks (ages are between ≈3000 and 12,000 years [15,25]) prevents application of even shorter-lived decay systems (e.g. ^{230}Th–^{226}Ra). Previously determined major element, trace element, radiogenic isotope and U–Th disequilibrium data on the same samples were presented in Slater et al. [15,25] and Stracke et al. [16,17].

(^{230}Th/^{238}U) ratios in basalts from Theistareykir have a relatively large range (1.12–1.41; [17]), but do not correlate with (^{231}Pa/^{235}U) ratios (1.83–2.71; Table 2 and Fig. 2). For a given set of D_U, D_{Th}, and D_{Pa} values, ^{230}Th and ^{231}Pa excesses decrease with increasing upwelling rate (W) and porosity (ϕ) and decreasing melt extraction velocity (v; Fig. 2). Variation of one of these parameters while keeping the other two constants affects the (^{230}Th/^{238}U) and (^{231}Pa/^{235}U) ratios in the same direction, i.e. (^{230}Th/^{238}U) and (^{231}Pa/^{235}U) ratios either increase or decrease (solid gray grid lines in Fig. 2). Therefore, variation of W, v, or ϕ alone leads to arrays with a positive slope in a (^{231}Pa/^{235}U)–(^{230}Th/^{238}U) diagram (the same holds for (^{226}Ra/^{230}Th) versus (^{230}Th/^{238}U); see discussion in Section 4).

If increasing upwelling rates (W) are coupled to even greater increases in melt extraction velocities (v), calculated trends with a shallow positive or almost horizontal slope result in a (^{231}Pa/^{235}U) versus (^{230}Th/^{238}U) diagram (Fig. 2a). While the absolute values of v and W are dependent on the selected partition coefficient values (see discussion in Section 5), an increase of v/W as a function of W is required, and this empirical relationship is a robust feature that persists independent of the selected mineral-melt partition coefficients.

Table 2
Pa measurements in the Theistareykir samples

Sample	Pa (fg/g)	$\left(\frac{^{238}U}{^{232}Th}\right)$	$\left(\frac{^{230}Th}{^{232}Th}\right)$	$\left(\frac{^{230}Th}{^{238}U}\right)$	$\left(\frac{^{231}Pa}{^{235}U}\right)$	±2σ
Storaviti						
9330	31.3	0.945	1.128	1.194	1.889	0.079
9385	18.5	0.921	1.173	1.273	1.917	0.040
9389	16.9	0.900	1.151	1.279	1.853	0.031
Bondholshraun						
9333	27.2	0.951	1.210	1.273	2.076	0.048
9499	27.1	0.950	1.210	1.274	2.086	0.027
Bogarhraun						
9309	19.9	0.930	1.275	1.371	2.112	0.043
9313	16.1	0.885	1.220	1.378	2.119	0.037
9409	17.5	0.979	1.191	1.216	2.116	0.076
Langavitihraun						
9356	13.2	1.024	1.342	1.311	2.710	0.110
9394	16.2	0.967	1.245	1.287	2.411	0.077
94112		0.894	1.227	1.372	2.008	
Arnavamurhraun						
9371	14.7	0.861	1.122	1.303	1.825	0.026
Hoefuheidharmuli						
9370	11.6	0.876	1.088	1.242	2.042	0.062
9383	40.4	0.943	1.19	1.262	2.188	0.053

Pa concentrations were determined at the Institute du Physique du Globe (IPGP) using the techniques described in Bourdon et al. [26,73]. The used ^{233}Pa spike was calibrated against LV18, a 1 Ma old rhyolithic glass with (^{231}Pa/^{235}U)=1 [73]. See Bourdon et al. [26,73] for further details of the analytical technique. U–Th data are taken from Stracke et al. [17].

For given upwelling rates (W), calculated values of melt extraction velocities (v) in Fig. 2a also depend on the selected porosity (ϕ) (v increases with increasing ϕ; compare Fig. 2a and b). With the partition coefficient values used here and for residual porosities greater than 0.1%, calculated melt extraction velocities roughly correspond to estimates by Maclennan et al. [10] (v>50 m/yr; Fig. 2a and b). The increase in melt extraction velocity with increasing upwelling velocity required by the Theistareykir data suggests that pulses of fast upwelling velocity (i.e. high melt productivity) correspond to pulses of fast melt extraction. This scenario is supported by the observation that high melt eruption (extraction) rates occur at times of high melt productivity (i.e. fast upwelling rates; [10]). Geological observations and geochemical data are therefore readily explained by faster melt extraction at periods of higher

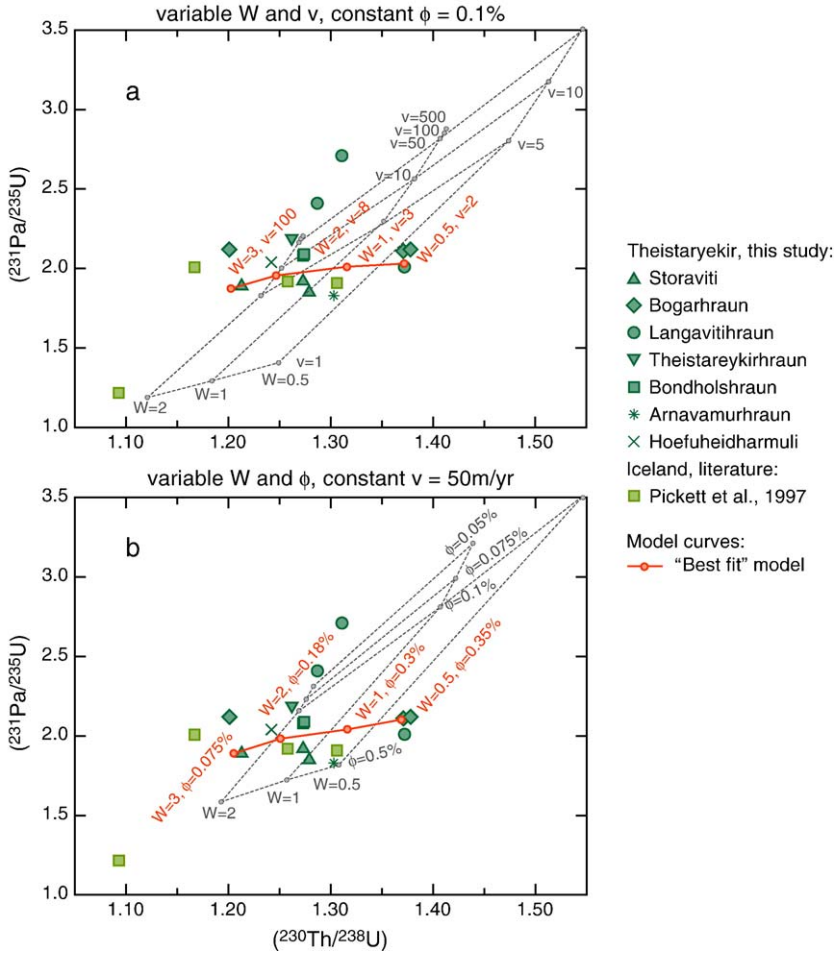

Fig. 2. Plot of (^{231}Pa/^{235}U) versus (^{230}Th/^{238}U) in Theistareykir basalts plus calculated variations in ^{231}Pa and ^{230}Th excess as a function of upwelling rate (W [cm/yr]) and melt extraction velocity (v [m/yr]) in (a), and upwelling rate (W) and porosity (ϕ [%]) in (b). The data are divided into samples from one eruption event. Red curves in (a) and (b) are "best-fit" models using variables W and v (a) and variables W and ϕ (b). Calculations are done using the model described in detail in Stracke et al. [17] assuming a degree of melting of 15%, an initial depth of melting of 100 km and melt transport to the base of the lithosphere at 10 km.

melt production due to higher upwelling rates, supporting the idea that melt transport could be episodic.

If, instead, U–Th–Pa data at Theistareykir are explained by dynamic melting with variations in upwelling rate (W) and residual porosity (ϕ) ,*decreasing* ϕ with increasing W (i.e. increasing melt productivity) is required (Fig. 2b). In contrast to increasing extraction velocities with increasing upwelling rates, however, there is no observation or obvious physically and geologically plausible explanation for *decreasing* porosity with increasing upwelling rate, i.e. *lower* threshold porosities at higher melt production rates.

In summary, the picture that emerges from the U–Th–Pa systematics at Theistareykir is one of episodic melting with a general trend of increasingly faster melt extraction rates at times of higher melt productivity (higher upwelling rates). Superimposed on this general trend are occasional short-pulsed excursions of melts that are extracted exceptionally fast (two samples with the highest excess ^{231}Pa in Fig. 2a).

4. U–Th–Pa–Ra characteristics of global MORB and OIB

In OIB, (^{231}Pa/^{235}U) and (^{230}Th/^{238}U) ratios correlate positively. In MORB, there is a general lack of correlation between ^{230}Th and ^{231}Pa excess, although some systematic variation exists in individual sample suites (Fig. 1). For a given (^{230}Th/^{238}U) ratio, MORB have higher excess ^{231}Pa than OIB, with only slight overlap, resulting in two distinct arrays of MORB and OIB in a (^{231}Pa/^{235}U) versus (^{230}Th/^{238}U) diagram (Fig.

1a and b, see also [26,27]). There is a rough positive trend of ^{230}Th–^{226}Ra excesses in OIB, whereas MORB show a distinct negative correlation. Over the entire spectrum of excess ^{230}Th, (^{226}Ra/^{230}Th) ratios in OIB tend to be lower than those in MORB (Fig. 1c and d).

The ^{230}Th–^{231}Pa–^{226}Ra data in OIB have been explained with standard models [22,28] by variation in upwelling velocity (W) and/or residual porosity (ϕ) (e.g. [26,29,30]). In detail, however, it is often impossible to find a combination of W and ϕ values that explain the combined ^{230}Th–^{231}Pa–^{226}Ra relationships (Fig. 1, see also discussion in Sims et al. [29]). Also, the almost constant ^{231}Pa excess for variable ^{230}Th and ^{226}Ra excesses observed in some MORB suites (e.g. [31]), the difference between the MORB and OIB array in a (^{231}Pa/^{235}U) versus (^{230}Th/^{238}U) diagram (Fig. 1 a and b), and the inverse relationship between ^{230}Th and ^{226}Ra excesses in MORB (Fig. 1c and d) cannot be explained with dynamic melting with infinite melt transport velocities [22] or the equilibrium transport model [28].

Recently, more complicated melt extraction models have therefore been proposed, arguing for differences in melt migration processes at different depths/pressure in the mantle (e.g. [8,31–33]). In these "two-porosity" models, shallow melts travel slowly by porous flow and mix with fast traveling melts extracted through high-porosity channels from greater depth. Alternatively, models calling for diffusive interaction between extracted melts and cumulates in the crust–mantle transition zone [34] have been used to argue that processes other than melting and melt migration may influence the U–Th–Ra systematics in MORB and OIB.

In the following we will show that the U–Th–Pa–Ra data in MORB and OIB can be adequately modeled using dynamic melting with finite melt transport time; a model that effectively simulates melt extraction without chemical equilibrium between melt and matrix, i.e. melt flow in a channeled network. The successful solutions lead to an empirical relationship between W, v and ϕ derived from the U–Th–Pa–Ra systematics in oceanic basalts. Finally, the possible influence of variations in mineral-melt partitioning on the U–Th–Pa–Ra data in oceanic basalts and the constraints on melt extraction velocities will be discussed.

4.1. U–Th–Pa–Ra characteristics of MORB

Using dynamic melting with a given set of D_U, D_{Th}, and D_{Pa} values, variation of either upwelling velocity (W), melt extraction velocity (v), or porosity (ϕ) alone leads to arrays with a positive slope in a (^{230}Th/^{238}U) versus (^{231}Pa/^{235}U) diagram (solid gray grid lines in Figs. 1 and 2; see discussion above). Fast melt velocity (v) and low porosity (ϕ) lead to large excess ^{226}Ra excess ^{231}Pa and ^{230}Th but (^{226}Ra/^{230}Th) ratios are virtually independent of variations in upwelling velocity (Fig. 1a–d). Changes in v at constant ϕ (or vice versa) therefore also result in arrays with a positive slope in a (^{226}Ra/^{230}Th)–(^{230}Th/^{238}U) diagram (Fig. 1c and d; solid gray grid lines). Variations in only one of the critical melting parameters (W, v, and ϕ) while keeping the other two parameters constant thus leads to positively sloped arrays in (^{231}Pa/^{235}U) and (^{226}Ra/^{230}Th) versus (^{230}Th/^{238}U) diagrams and can therefore not explain the negative relationship between (^{226}Ra/^{230}Th) and (^{230}Th/^{238}U) observed in MORB (Figs. 1–3).

The same holds for the equilibrium transport model [28]. Note, however, that W, v and ϕ are directly related in the equilibrium transport model by $v = \rho_s WF/\rho_f\phi$ (with F = degree of melting, ρ_s and ρ_f are the densities of solid and melt, respectively). Adjustable parameters are W and ϕ only [35] so that changes in v cannot be modeled independently, which makes it difficult to attribute changes in excess ^{230}Th, ^{231}Pa and ^{226}Ra uniquely to W, v, or ϕ. Note also that this relationship is only valid for a 1-D, steady-state melting column and does not apply to a 2-D or an episodic melting regime.

It follows from the above discussion that systematic variation between two or three parameters (W, v or ϕ) is required to account for the U–Th–Pa–Ra characteristics in MORB. Excess ^{230}Th and ^{231}Pa are most sensitive to upwelling rates (W) and are significantly affected by melt extraction velocity (v) and porosity (ϕ). Excess ^{226}Ra, on the other hand, are primarily influenced by v and ϕ. Therefore, the number of parameters that determine the *combined* ^{226}Ra, ^{231}Pa and ^{230}Th excess in MORB can be narrowed down from three to two. Since only changes in upwelling velocity (W) can explain the considerable spread of the (^{230}Th/^{238}U) ratios in both MORB and OIB, these two parameters must either be W and v, or W and ϕ.

Similar to the scenario discussed for Theistareykir, increasing upwelling velocity (W) coupled to substantial increases in melt extraction velocity (v) leads to lower (^{230}Th/^{238}U) ratios and progressively higher ^{226}Ra excesses while maintaining similar (^{231}Pa/^{235}U) ratios. As a consequence, arrays with a shallow positive or almost horizontal slope in a (^{231}Pa/^{235}U) versus (^{230}Th/^{238}U) diagram and negatively sloped arrays in a (^{226}Ra/^{230}Th) versus (^{230}Th/^{238}U) plot result from mixing between melts created with different v/W ratios (Fig. 3a–d). The high absolute values of (^{231}Pa/^{235}U) for relatively small values of excess ^{230}Th in the EPR-

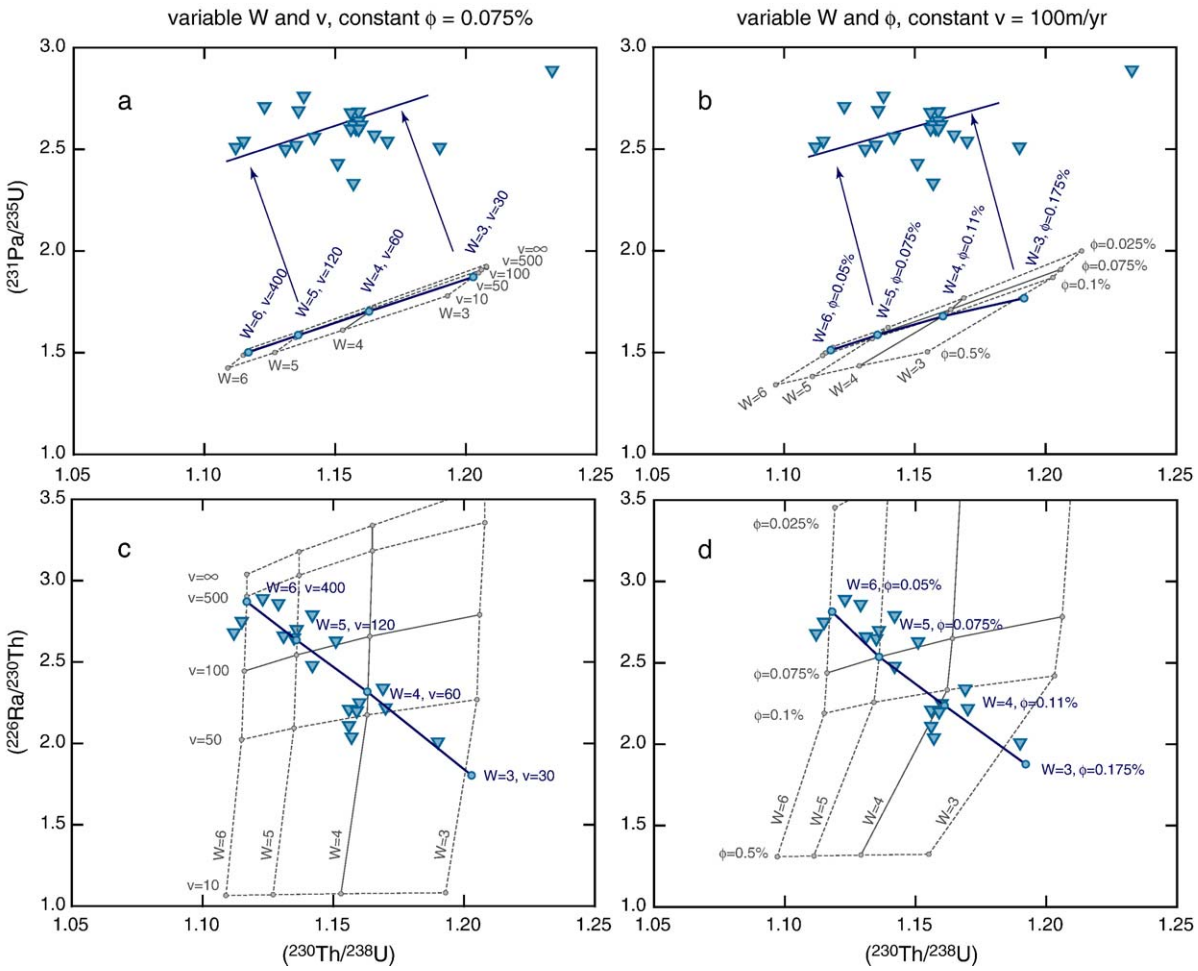

Fig. 3. Plot of (a) and (b) (^{231}Pa/^{235}U) versus (^{230}Th/^{238}U) and (b) and (d) (^{226}Ra/^{230}Th) versus (^{230}Th/^{238}U) in MORB from the East Pacific Rise (EPR) from 9 to 10°N [31,77] compared to the calculated ^{230}Th–^{231}Pa–^{226}Ra excesses as a function of W [cm/yr], v [m/yr] and ϕ [%]. The negative (^{226}Ra/^{230}Th)–(^{230}Th/^{238}U) array of the EPR-MORB can be explained with coupled changes in v and W (c), or ϕ and W (b and d; solid blue lines). The calculated shallow positive arrays in (a) and (b) lie at lower (^{231}Pa/^{235}U) than observed in the EPR-MORB, which might be due to too small D_U values. See text for detailed discussion. Model parameters are similar to those described in Fig. 1.

MORB, and MORB in general are, however, difficult to explain with the partition coefficient values used in the calculations in Figs. 1–4 (see Figs. 1a,b, 4a,b and discussion below).

If, instead of variations in upwelling and melt extraction velocity, U–Th–Pa–Ra data in MORB are explained by dynamic melting with variations in upwelling velocity (W) and porosity (ϕ), the negative trend between ^{226}Ra and ^{230}Th excesses require increasing W and *decreasing* ϕ (Fig. 3b and d). However, increasing upwelling velocities (W) also lead to rapidly decreasing excess ^{231}Pa, which cannot be compensated by decreasing porosity (Fig. 3b). In addition, as discussed above, a physically and geologically plausible reason for decreasing porosity with increasing upwelling rate is lacking.

Passive mantle upwelling, as is typical for melting beneath ridges, leads to large across-axis variations in upwelling rate (W). W decreases with increasing distance from the ridge axis [6]. The slower W away from the ridge axis leads to larger excess ^{230}Th and ^{231}Pa in the instantaneous melts compared with melts generated closer to the ridge axis. Preservation of these initially large excesses requires high melt transport velocities (v), or short melt transport time. The relationship between excess ^{230}Th, ^{231}Pa, and ^{226}Ra in melts created at different distances to the ridge axis therefore depends strongly on the ratio of melt extraction velocity (v) to the upwelling velocity (W).

The ^{230}Th–^{231}Pa–^{226}Ra data in MORB, i.e. the inverse relationship between excess ^{226}Ra and ^{230}Th and the concomitant small variation in excess ^{231}Pa, are

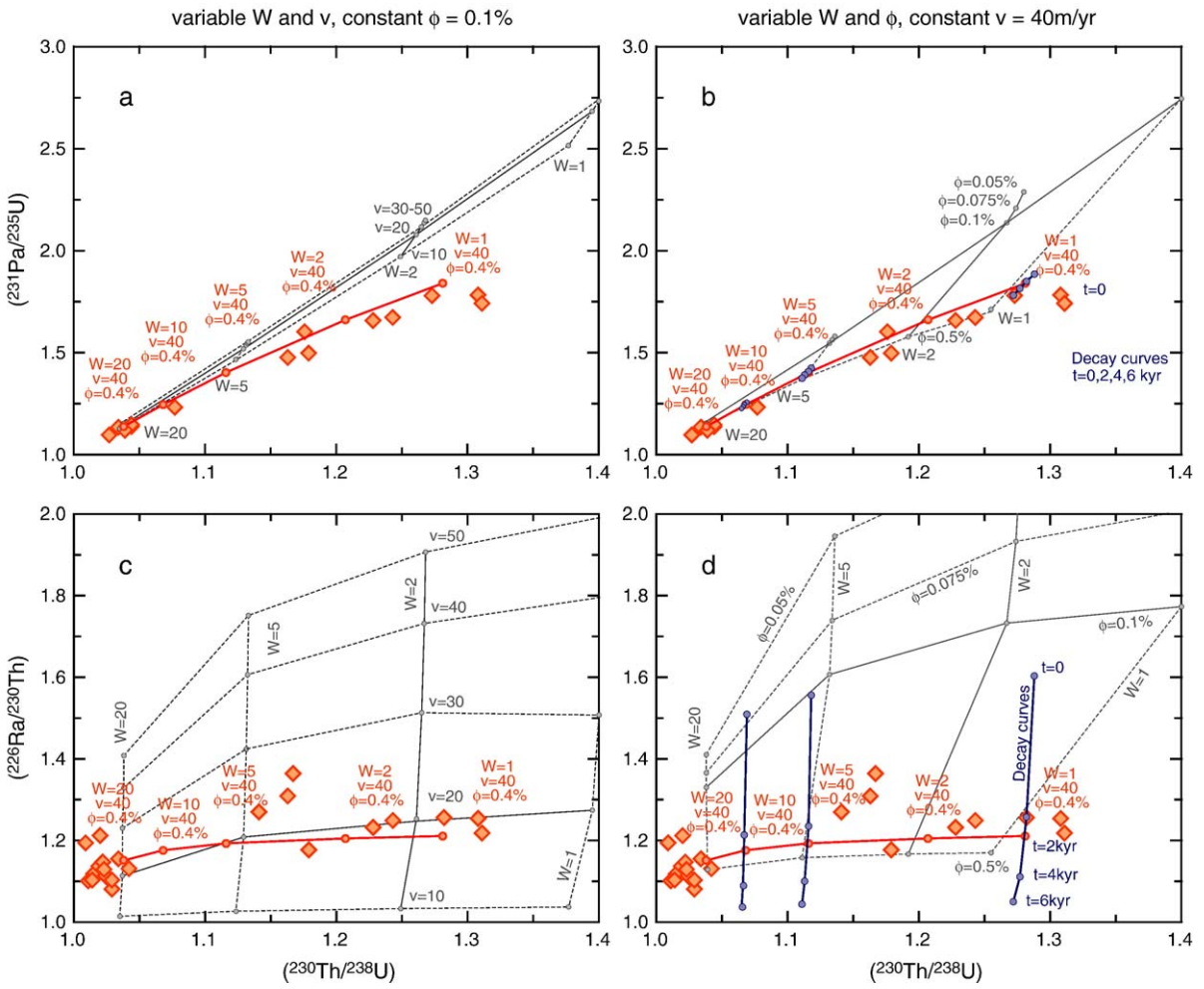

Fig. 4. Plot of (a) and (b) (^{231}Pa/^{235}U) versus (^{230}Th/^{238}U) and (b) and (d) (^{226}Ra/^{230}Th) versus (^{230}Th/^{238}U) in Hawaiian basalts [29–31,36,78] compared to the calculated ^{230}Th–^{231}Pa–^{226}Ra excesses as a function of W [cm/yr], v [m/yr] and ϕ [%]. Decay curves for radioactive decay during magma storage for samples extracted with infinite melt extraction velocity are also plotted using increments of 2000 years (blue curves in b and d; W=1, 5 and 10 cm/yr, and ϕ=0.4%). Red curves are "best-fit" models using variable W but constant v and ϕ. See text for detailed discussion. Calculations are done assuming a degree of melting of 5% and an initial depth of melting of 120 km and melt extraction distances of 100 km.

readily explained by mixing between melts created at variable distances to the ridge axis if the melts generated close to the ridge axis travel significantly faster than the melts created farther from the ridge axis (Fig. 3 blue curves). Of course, melts created far from the ridge axis travel over greater distances than melts created close to the ridge axis. So for equal melt extraction velocity (v), melt transport time increases with increasing distance to the ridge axis and the apparent velocity increase suggested in Fig. 3a and b could also be simply due to longer melt travel distances.

The scenario suggested above to explain the U–Th–Pa–Ra data in MORB also leads to systematic changes in the trace element composition of the erupted melts and can thus be tested independently using other geochemical parameters. The only published MORB dataset with a complete set of U–Th–Pa–Ra data, and major, trace element and radiogenic isotope data determined on the same samples is for basalts from the East Pacific Rise (EPR) at 9–10°N [31]. For the EPR-MORB, higher excess ^{230}Th is coupled to lower degrees of melting (F; increasing La/Yb, Na, decreasing Mg# and $\alpha_{(Sm/Nd)}$ [31]). Increasing (^{230}Th/^{238}U) with decreasing F is therefore consistent with the low-F, high-^{230}Th excess melts being generated farther from the ridge axis than are the high-F, low-^{230}Th excess melts. If the U–Th–Pa–Ra data are explained by variations in upwelling rate (W) and porosity (ϕ), lower ϕ and higher W are needed to account for the large excess ^{226}Ra of melts with low (^{230}Th/^{238}U) ratios. This

would indicate that porosity decreases towards the ridge axis (higher W); a scenario for which there is no obvious physical or geological explanation.

The U-series and other geochemical data in MORB are therefore best explained by mixing of melts generated at different lateral distances to the ridge axis where the melts generated close to the ridge axis travel significantly faster and are generated with faster upwelling velocity than melts created farther from the ridge axis.

4.2. U–Th–Pa–Ra characteristics of OIB

In contrast to MORB, OIB form positive arrays in (^{231}Pa/^{235}U) versus (^{230}Th/^{238}U) and to a lesser degree in (^{226}Ra/^{230}Th) versus (^{230}Th/^{238}U) space (Fig. 1). These trends have been explained by variation in upwelling rate (W) and porosity (ϕ) using both dynamic melting and equilibrium porous flow models (discussion above, see also [26,27,29,30,36–39]). However, when using dynamic melting with infinite melt transport time (v) or equilibrium porous flow (e.g. [28]), calculated excess ^{226}Ra is often far too high for successfully modeled (^{231}Pa/^{235}U) and (^{230}Th/^{238}U) ratios, irrespective of the selected partition coefficients (see also discussion in Sims et al. [29]).

In contrast, dynamic melting with constant, but *finite* melt transport velocity, constant porosity (ϕ) and variable upwelling rates (W) can successfully explain the combined ^{230}Th–^{231}Pa–^{226}Ra excesses in OIB (Fig. 4; solid red lines). Thus, the fundamental difference between melting at ridges and ocean islands is that OIB melting is dominated by variation in upwelling rate only, whereas melting at ridges requires systematic variation in at least two melting parameters (most likely W and v, see discussion in Section 4.1). Assuming infinite melt extraction velocities, the observed low (^{226}Ra/^{230}Th) ratios in OIB (relative to (^{231}Pa/^{235}U)) could alternatively be due to decay of excess ^{226}Ra (and to a much lesser degree of ^{231}Pa and ^{230}Th) during magma storage (Fig. 4b and d).

In contrast to melting beneath ridges, melting beneath ocean islands occurs by active upwelling. Increasing temperature towards the center of large plumes is expected to result in a pattern of more or less concentrically increasing upwelling rates (e.g. [40–42]), which has been suggested to be responsible for the observed U-series disequilibrium patterns in erupted lavas from Iceland, Hawaii and the Azores [6,29,30,39,43,44]. The observed positive global OIB arrays are therefore expected to originate from superimposed global variations in upwelling velocity due to different buoyancy fluxes (i.e. upwelling rate; [26]) and local variation in upwelling velocities as a function of radial distance from the plume center.

5. The influence of mineral-melt partitioning

5.1. Influence of mineral-melt partition coefficients on U-series disequilibrium

Any value inferred for upwelling rate (W), melt extraction velocity (v) and porosity (ϕ) from U-series data in MORB and OIB depends strongly on the selected U–Th–Pa–Ra mineral-melt partition coefficients. Based on experimentally and theoretically estimated mineral-melt partition coefficients (Blundy and Wood [45] and references therein; Table 3 supplementary material), it is generally assumed that the values of the bulk U, Th, Pa and Ra partition coefficients (D_U, D_{Th}, D_{Pa}, and D_{Ra}) follow the order $D_U > D_{Th} > D_{Pa} > D_{Ra}$ for melting in the garnet-stability field. U, Th, Pa and Ra are all highly incompatible elements (D_U, D_{Th}, D_{Pa}, and $D_{Ra} < 0.01$), with values of D_{Pa} and D_{Ra} approaching 0 [45]. Calculated ^{230}Th, ^{231}Pa, and ^{226}Ra excesses depend on both the absolute values and the ratios of the respective D_U, D_{Th}, D_{Pa}, and D_{Ra} values.

(^{230}Th/^{238}U) ratios increase with increasing D_U/D_{Th} (for a melt fraction less than D_U). For lower values of D_U and D_{Th}, lower excess ^{230}Th results for constant D_U/D_{Th} ratios. (^{231}Pa/^{235}U) ratios depend on D_U/D_{Pa}, but based on the assumption that Pa is almost perfectly incompatible [45], variations in D_U/D_{Pa} are caused only by variations in D_U. (^{231}Pa/^{235}U) ratios in the melt increase with increasing D_U. Similarly, because D_{Ra} values are effectively close to 0 [45], variations in D_{Th}/D_{Ra} are caused mainly by variations in D_{Th}. (^{226}Ra/^{230}Th) ratios increase with increasing D_{Th}.

Note that some observations are difficult to explain by starting melting in the garnet-stability field and continued melting in the spinel-stability field as assumed for the calculations in the previous discussion (e.g. Figs. 1–4). Especially the high excess ^{226}Ra and ^{231}Pa in MORB with (^{230}Th/^{238}U) close to 1 (e.g. [46–48]; Fig. 5) are practically impossible to model with this scenario, independent of the selected melting parameters (W, v and ϕ). The low (^{230}Th/^{238}U), high (^{226}Ra/^{230}Th) and (^{231}Pa/^{235}U) ratios in MORB therefore require melting with different partition coefficients, i.e. D_U/D_{Th} ratios of about 1 and higher average D_U/D_{Pa} and D_{Th}/D_{Ra} ratios than those used in the calculations in Figs. 1–4. In addition, the consistently higher excess ^{231}Pa in MORB compared to OIB suggest that melting at ridges

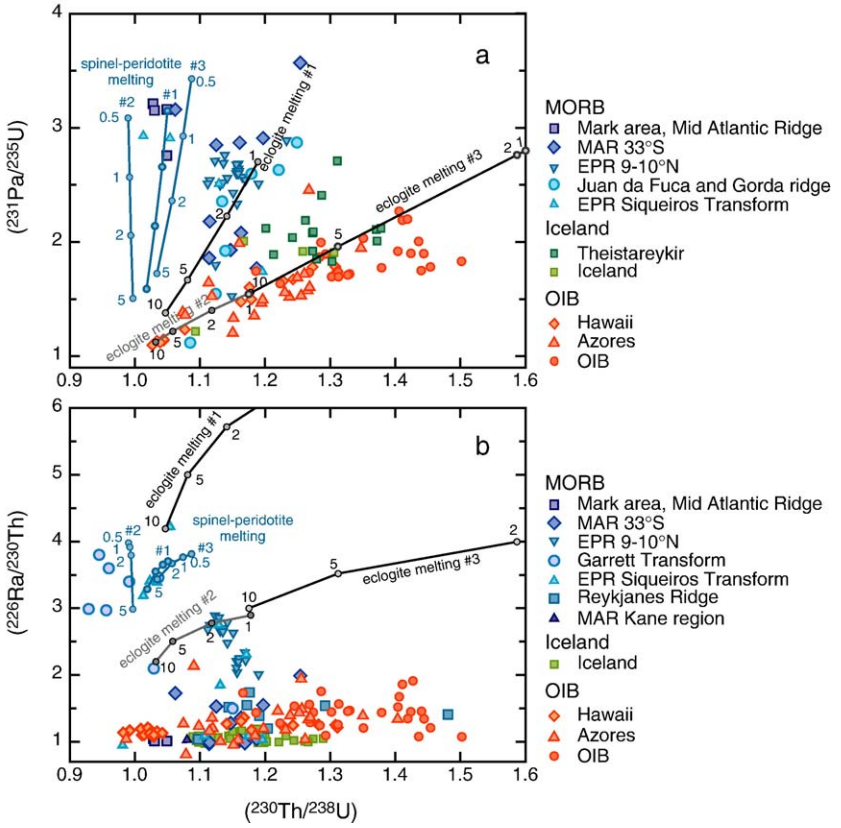

Fig. 5. Plot of (a) (^{231}Pa/^{235}U) versus (^{230}Th/^{238}U) and (b) (^{226}Ra/^{230}Th) versus (^{230}Th/^{238}U) in MORB and OIB. Also shown are calculated model curves for partial melting of spinel peridotite in blue and eclogite/pyroxenite in black, respectively. U and Th partition coefficients used for modeling spinel peridotite are taken from Salters et al. [52] and McDade et al. [51] for olivine and orthopyroxene and from Salters et al. [52], McDade et al. [51] and Wood et al. [59] for clinopyroxene in spinel peridotite #1, #2 and #3, respectively (see Table 3). Melting of spinel peridotite (blue curves) is done with residual porosity of 0.15% for spinel peridotite #2 and a residual porosity of 0.2% for spinel peridotite #1 and #3 and assumes *infinite* melt extraction velocities and a degree of melting of 10%. Tick marks indicate upwelling rate in cm/yr. The modal composition of the spinel peridotite is given in Table 1. Melting of eclogite (black curves) is done with 3 different sets of U and Th partition coefficients: for eclogite #1 clinopyroxene and garnet partition coefficients from Klemme [56] are used, whereas for eclogite #2 and #3, cpx and garnet partition coefficients from Pertermann et al. [55,58] are used. Differences in the calculated curves for eclogite #2 and #3 are due to using different garnet partition coefficient for low Ti and high Ti garnet from Pertermann [55] (see also Table 3). For eclogite melting a residual porosity of 0.1%, infinite melt transport times and a degree of melting of 10% are used and a modal composition of 75% clinopyroxene and 25% garnet (see discussion in Pertermann [55] for appropriate mineral modes). Data sources as given in Fig. 1.

in general is likely to occur with higher average D_U/D_{Pa} ratios than melting at ocean islands.

Differences in bulk partition coefficient values (D's) during melting beneath ridges and ocean islands can either be due to melting of sources with different mineralogical composition or due to pressure-dependent changes in mineral-melt partition coefficients during progressive melting (e.g. [45,49–51]). Pressure-dependent changes in D's are implemented in the dynamic melting model used here [17]. U, Th, Pa and Ra are all highly incompatible elements that are exhausted from the residual mantle after less than about 2–5% of melting. As a consequence, for dynamic melting, the first stages of melting are most critical for the resulting U-series characteristics of the erupted melts. In contrast to the equilibrium transport model, pressure-dependent changes in D values thus have little influence, unless melting starts close to the spinel–garnet transition (see Fig. 4 in [17]). For dynamic melting, different source lithologies are therefore required to explain the high (^{226}Ra/^{230}Th) and (^{231}Pa/^{235}U) and low (^{230}Th/^{238}U) ratios of some MORB (e.g. [46–48]; Fig. 5).

5.2. Peridotite versus eclogite/pyroxenite melting

Owing to the compositional dependence of mineral-melt partition coefficients (D), mineral-melt D values for peridotite and eclogite/pyroxenite are likely to be

different. Experimentally determined mineral-melt partition coefficients for garnet (D_{gt}) are dependent on melt composition [52] as well as pressure and temperature of melting [50,52] and the garnet composition [53–55]. Van Westrenen et al. [53,54] observed D_{gt} to increase with increasing Ca content, but this observation was not confirmed by a comparable subsequent study [56]. Pertermann et al. [55], on the other hand, have observed increasing D_{gt} with decreasing Ti contents. Thus, the differences in D_{gt} due to different garnet composition and the different modal abundances of cpx and garnet in eclogites and peridotites potentially result in a different partitioning behavior of trace elements during partial melting. The potential implications of such effects were first discussed for the U-series by Stracke et al. [57] and subsequently by Bourdon and Sims [27]. Recent experiments postdating the Stracke et al. [57] study have shown, however, that the expected increase in D_{gt} due to the higher Ca contents [53,54] could be compensated by the higher Ti content for eclogitic compared to peridotitic garnets [55].

For a given eclogite/pyroxenite, the calculated bulk D_U/D_{Th} ratio depends on both the respective D_U/D_{Th} ratios and the absolute values of $D_{U,Th}$ in cpx and garnet ($D_{U,Th\ gt}$, $D_{U,Th\ cpx}$). Although there is some variation in the D_U/D_{Th} ratios in cpx, most D_U/D_{Th} ratios in cpx are close to 1, whereas all D_U/D_{Th} ratios in garnet are significantly greater than 1. Thus, among the common peridotite and eclogite/pyroxenite minerals, cpx has the lowest and garnet the greatest potential for fractionation of Th from U (Table 3 supplementary material). The higher the absolute values of the mineral-melt partition coefficients in cpx relative to garnet, and the higher the modal abundance of cpx compared to garnet, therefore, the smaller is the magnitude of U and Th fractionation during partial melting, and the smaller are the observed ^{230}Th excesses.

$D_{U,Th\ gt}$ and $D_{U,Th\ cpx}$ vary by about two orders of magnitude (Table 3 supplementary material). If only the mineral-melt partition coefficients from recent experiments that are most appropriate for eclogite melting are considered, $D_{U,Th\ gt}$ varies by two orders of magnitude, whereas $D_{U,Th\ cpx}$ varies by a factor of two to three (Table 3 supplementary material). The potential of eclogite/pyroxenite for fractionation of U and Th and thus for generation of large ^{230}Th excesses during partial melting consequently depends strongly on the selected $D_{U,Th\ gt}$. Calculated *bulk* D_U/D_{Th} ratios for eclogite/pyroxenite range roughly from values slightly above 1 (corresponding to eclogite #1 and 2 in Fig. 5), which are similar to bulk D_U/D_{Th} ratios for eclogite/pyroxenite determined by Stracke et al. [57] and Bourdon and Sims [27], to values similar to those typical for garnet peridotites (corresponding to eclogite #3 in Fig. 5; [54,55,57]). As a consequence, the ability of eclogite/pyroxenite to fractionate U from Th and to generate large ^{230}Th excess remains difficult to evaluate and precludes any definite conclusion, either in favor of, or against, the ability to generate large ^{230}Th excesses by partial melting of eclogite/pyroxenite (Fig. 5).

Recent partitioning experiments by Pertermann et al. [55,58], however, suggest that the magnitude of Th and U fractionation during partial melting of eclogite/pyroxenite and garnet peridotite can be similar, leading to similar ^{230}Th excesses in derivative melts. In this case, partial melting of eclogite/pyroxenite and garnet peridotite is difficult to distinguish based on U-series data alone. This could explain why at Theistareykir, the combined Sr, Nd, Hf and Pb isotope and major and trace element data provide evidence for melting of low melting temperature components (possibly eclogite/pyroxenite or enriched peridotite [16]) but neither the (^{231}Pa/^{235}U) nor the (^{230}Th/^{238}U) ratios in the Theistareykir basalts generally correlate with other isotope ratios (Sr, Nd, Hf or Pb) or trace element and major element parameters indicative of the inferred low melting temperature component [16,17].

5.3. Melting of spinel peridotite

MORB with high ^{231}Pa and ^{226}Ra but low ^{230}Th excesses (e.g. [46–48]; Fig. 5) require melting with average bulk D_U/D_{Th} ratios of about 1, and high absolute values of D_U and D_{Th} (Sections 5.1 and 5.2). On the basis of the discussion above and from Table 3 it is obvious that partial melting in the presence of garnet, either in form of melting garnet-peridotite or eclogite/pyroxenite, causes substantial fractionation of U and Th, which, depending on the melting conditions, can translate into large excess ^{230}Th. For the cases where selected $D_{U,Th\ gt}$ are smaller than $D_{U,Th\ cpx}$, however, melting of eclogite/pyroxenite can have the appropriate bulk D values to generate low ^{230}Th but high ^{231}Pa and ^{226}Ra excesses (Fig. 5; see also discussion above and [27,57]). Since this is by no means the general case for melting of eclogite/pyroxenite, the role of eclogite/pyroxenite for generating low (^{230}Th/^{238}U), but high (^{231}Pa/^{235}U) and (^{226}Ra/^{230}Th) ratios remains somewhat ambiguous (Fig. 5). Melting of garnet peridotite, on the other hand, is clearly not suitable for generating melts with low (^{230}Th/^{238}U) ratios but high excess ^{226}Ra and ^{231}Pa (Fig. 1).

The only lithologies for which, in general, relatively small U and Th fractionation could be asserted with a

high degree of confidence are therefore garnet-free rocks. For melting beneath mid-ocean ridges the obvious candidate is spinel peridotite. Selecting mineral-melt partition coefficients that are most appropriate for melting spinel peridotite at low pressure [51,52,59] indeed results in low excess ^{230}Th, or even excess ^{238}U, and high (^{226}Ra/^{230}Th) and (^{231}Pa/^{235}U) ratios similar to those observed in some MORB (e.g. [46–48]; Fig. 5). The low bulk D_U/D_{Th} of the spinel peridotite cause the small excesses or deficiencies of ^{230}Th, whereas the high bulk D_U and D_{Th} ratios are responsible for the large ^{226}Ra and ^{231}Pa excesses. Note, however, that for D_{cpx} values similar to those derived in partitioning experiments (Table 3 supplementary material), relatively slow upwelling velocities (about 1–2 cm/yr) and rapid, near infinite, melt extraction velocities are required to produce and preserve the high (^{226}Ra/^{230}Th) and (^{231}Pa/^{235}U) ratios (Fig. 5). In order to maintain the large ^{226}Ra and ^{231}Pa excesses at higher upwelling velocities, D_{cpx} values greater than those measured in any appropriate experimental study (Table 3) are required to compensate for the small amount of excess daughter elements (^{226}Ra and ^{231}Pa) produced by decay during fast upwelling. Melting of spinel peridotite at low average pressure with slow upwelling velocities is a direct consequence of progressive melting beneath ridges and is consistent with the origin of the basalts from the Garrett and Siqueiros Transform [46,48], which have among the highest excess ^{231}Pa and ^{226}Ra for given (^{230}Th/^{238}U) ratios of MORB in general (Fig. 5). Moreover, the relatively high D_{cpx} values required for the high (^{226}Ra/^{230}Th) and (^{231}Pa/^{235}U) ratios and the observation that high (^{226}Ra/^{230}Th) and (^{231}Pa/^{235}U) ratios are either accompanied by small ^{230}Th excesses or deficits (see also [60,61]) are also consistent with the observation that D_{cpx} increase and the sense of U and Th fractionation reverses with decreasing pressure (e.g. [45,49–51]).

6. Constraints on melt extraction velocities

Absolute values for melt extraction times are hard to quantify with U–Th–Pa–Ra data alone. On the one hand this is due to the uncertainties imposed by the partition coefficient values, and on the other hand because the calculated melt extraction velocity depends on the selected residual porosity (compare Figs. 1 and 3). Dependent on the ^{230}Th–^{231}Pa–^{226}Ra excesses and the selected partition coefficients and residual porosity values, melt extraction velocities on the order of a few 10 to well in excess of 100 m/yr, and up to infinite values for MORB with the highest ^{226}Ra excess ((^{226}Ra/^{230}Th) ≥ 2.5), are suggested in Figs. 1–5. These fast melt extraction velocities require channeled melt flow [6]. Note that calculated (^{226}Ra/^{230}Th) ratios for $v \geq 100$–500 m/yr rapidly approach those calculated for infinite melt extraction velocity (Figs. 1 and 3). More precise constraints on melt extraction velocity/time consequently require analyses of elements with shorter half-lives than ^{226}Ra ($t_{1/2} \sim 1600$ years), such as ^{210}Pb and ^{227}Ac ($t_{1/2} \sim 23$ and 22 years, respectively). A recent ^{210}Pb study [62] suggests melt extraction times on the order of 50–70 years (about 2–3 times $t_{1/2}$ ^{210}Pb) for the high ^{226}Ra and low ^{230}Th excess EPR-MORB ((^{226}Ra/^{230}Th) ≥ 2.5 and (^{230}Th/^{238}U) < 1.15), corresponding to melt extraction velocities on the order of 1–2 km/yr assuming melt travel distances ≤ 100 km. This is in good agreement with the results presented in this study (Figs. 3 and 5) and the short melt extraction times inferred by Claude-Ivanaj et al. [37] and for island arcs volcanics by Turner et al. [63,64]. It should be stressed, however, that the total observed variability in excess ^{226}Ra–^{231}Pa–^{230}Th in MORB and OIB demands considerable variability in melt extraction times, ranging from the extreme values that are too fast to allow for decay of ^{226}Ra in the MORB with the largest ^{226}Ra excesses [62] to values that lead to significant decay of ^{226}Ra for the majority of MORB and OIB (Figs. 1, 3 and 4).

7. Conclusions

Dynamic melting with finite melt transport velocity [17]), which effectively simulates melt transport without chemical equilibrium between melt and surrounding matrix, successfully explains the U-series systematics of the Theistareykir melts and those of oceanic basalts in general.

The ^{226}Ra–^{231}Pa–^{230}Th data in MORB are best explained by mixing of melts generated at different lateral distances to the ridge axis where the melts generated close to the ridge axis travel significantly faster and are produced with higher upwelling velocities than melts created farther from the ridge axis. At least intuitively, this scenario thus suggests a physical framework where melt extraction occurs in a fractal-tree pattern such that melt channels coalesce in progressively larger channels near the ridge axis (e.g. [65]). Global U-series systematics in OIB, on the other hand, originate from the superimposed variations in upwelling velocity due to global variation in buoyancy flux and local variation as a function of radial distance to the plume center. The U-series data therefore seem to indicate that melting and melt extraction follow a more

uniform and regular pattern at ocean islands than at ridges, which could provide important information for deciphering the underlying physics of melt extraction.

More complicated models for melting and melt transport (e.g. [8,31–33]) or diffusion-controlled models [34] are certainly viable. The successful modeling of the U–Th–Pa–Ra data in MORB and OIB with dynamic melting, however, shows that more complicated models are not required by the U-series systematics in oceanic basalts. The inferred rapid melt extraction times, the large compositional variability in melt inclusions [66–71] and the combined results of the Theistareykir study [9–17] are all most easily explained by channeled melt flow, and therefore suggest that channeled melt flow could be the general means of melt extraction in the Earth's mantle.

Acknowledgements

The authors would like to thank Ken Sims and an anonymous reviewer for their thoughtful reviews, Michael Bizimis for comments on earlier versions of this manuscript and Ken Farley for editorial handling.

Appendix A. Supplementary data

Supplementary data associated with this article can be found, in the online version, at doi:10.1016/j.epsl.2006.01.057.

References

[1] D. McKenzie, The generation and compaction of partially molten rock, J. Petrol. 25 (1984) 713–765.
[2] N.H. Sleep, Segregation of magmas from a mostly crystalline mush, Geol. Soc. Amer. Bull. 85 (1974) 1225–1232.
[3] V. Barcilon, F.M. Richter, Non-linear waves in compacting media, J. Fluid Mech. 164 (1986) 429–448.
[4] V. Barcilon, O. Lovera, Solitary waves in magma dynamics, J. Fluid Mech. 204 (1989) 121–133.
[5] C. Wiggins, M. Spiegelman, Magma migration and magmatic solitary waves in 3-D, Geophys. Res. Lett. 22 (1995) 1289–1292.
[6] C. Richardson, D. McKenzie, Radioactive disequilibria from 2D models of melt generation by plumes and ridges, Earth Planet. Sci. Lett. 128 (1994) 425–437.
[7] E. Aharonov, J. Whitehead, P.B. Kelemen, M. Spiegelman, Channeling instability of upwelling melt in the mantle, J. Geophys. Res. 100 (1995) 20433–420450.
[8] P.B. Kelemen, G. Hirth, N. Shimizu, M. Spiegelman, H.J.B. Dick, A review of melt migration processes in the adiabatically upwelling mantle beneath oceanic spreading ridges, Philos. Trans. R. Soc. Lond. Ser. A: Math. Phys. Sci. 355 (1997) 283–318.
[9] J. Maclennan, D. McKenzie, K. Groenvold, L. Slater, Crustal accretion under northern Iceland, Earth Planet. Sci. Lett. 191 (2001) 295–310.
[10] J. Maclennan, D. McKenzie, M. Jull, L. Slater, Link between volcanism and deglaciation in Iceland, Geochem. Geophys. Geosys. 3 (2002) 25.
[11] J. Maclennan, D. MCKenzie, F. Hilton, K. Gronvold, N. Shimizu, Geochemical variability from a single flow from northern Iceland, J. Geophys. Res. 108 (2003) 000121, doi:10.1029/2000JB000142.
[12] J. Maclennan, D. McKenzie, K. Groenvold, N. Shimizu, J. Eiler, N. Kitchen, Melt mixing and crystallization under Theistareykir, northeast Iceland, Geochem. Geophys. Geosys. 4 (11) (2003) 8624, doi:10.1029/2003GC000558.
[13] D. McKenzie, A. Stracke, J. Blichert-Toft, F. Albarede, K. Groenvold, K. O'Nions, Source enrichment processes responsible for isotopic anomalies in oceanic island basalts, Geochim. Cosmochim. Acta 68 (2004) 2699–2724.
[14] L. Slater, M. Jull, D. McKenzie, K. Gronvold, Deglaciation effects on mantle melting under Iceland: results from the northern volcanic zone, Earth Planet. Sci. Lett. 164 (1998) 151–164.
[15] L. Slater, D. McKenzie, K. Gronvold, N. Shimizu, Melt generation and movement beneath Theistareykir, NE Iceland, J. Petrol. 42 (2001) 321–354.
[16] A. Stracke, A. Zindler, V.J.M. Salters, D. McKenzie, J. Blichert-Toft, F. Albarède, K. Grönvold, Theistareykir revisited, Geochem. Geophys. Geosys. 4 (2003) 8507, doi:10.1029/2001GC000201 (pp. 000249).
[17] A. Stracke, A. Zindler, V.J.M. Salters, D. McKenzie, K. Groenvold, The dynamics of melting beneath Theistareykir, northern Iceland, Geochem. Geophys. Geosys. 4 (2003) 18. 8513, doi:10.1029/2002GC000347.
[18] F.A. Darbyshire, K. Priestley, R.S. White, R. Stefansson, G.B. Gudmundsson, S.S. Jakobsdottir, Crustal structure of central and northern Iceland from analysis of teleseismic receiver functions, Geophys. J. Int. 143 (2000) 163–184.
[19] J. Maclennan, D. McKenzie, K. Groenvold, Plume-driven upwelling under central Iceland, Earth Planet. Sci. Lett. 2001 (2002) 67–82.
[20] D. McKenzie, Constraints on melt generation and transport from U-series activity ratios, Chem. Geol. 162 (2000) 81–94.
[21] C.H. Langmuir, J.F. Bender, A.E. Bence, G.N. Hanson, S.R. Taylor, Petrogenesis of basalts from famous area — Mid-Atlantic Ridge, Earth Planet. Sci. Lett. 36 (1977) 133–156.
[22] D. McKenzie, ^{230}Th–^{238}U disequilibrium and the melting processes beneath ridge axes, Earth Planet. Sci. Lett. 72 (1985) 149–157.
[23] R.W. Williams, J.B. Gill, Effects of partial melting on the uranium decay series, Geochim. Cosmochim. Acta 53 (1989) 1607–1619.
[24] H. Zou, A. Zindler, Theoretical studies of ^{238}U–^{230}Th–^{226}Ra and ^{235}U–^{231}Pa disequilibria in young lavas produced by mantle melting, Geochim. Cosmochim. Acta 64 (2000) 1809–1817.
[25] L. Slater, Melt generation beneath Iceland, PhD. thesis, University of Cambridge, 1996.
[26] B. Bourdon, J.L. Joron, C. Claude-Ivanaj, C.J. Allegre, U–Th–Pa–Ra systematics for the Grande Comore volcanics: melting processes in an upwelling plume, Earth Planet. Sci. Lett. 164 (1998) 119–133.
[27] B. Bourdon, K.W.W. Sims, U-series constraints on intraplate basaltic magmatism, in: B. Bourdon, C. Lundstrom, G. Henderson, S.P. Turner (Eds.), U-series Geochemistry, vol. 52, Mineralogical Society of America, 2003, pp. 215–253.
[28] M. Spiegelman, T. Elliott, Consequences of melt transport for uranium series disequilibrium in young lavas, Earth Planet. Sci. Lett. 118 (1993) 1–20.

[29] K.W.W. Sims, D.J. DePaolo, M.T. Murrell, W.S. Baldridge, S.J. Goldstein, D. Clague, M. Jull, Porosity of the melting zone and variations in the solid mantle upwelling rates beneath Hawaii: inferences from ^{238}U–^{230}Th–^{226}Ra, and ^{235}U–^{231}Pa disequilibria, Geochim. Cosmochim. Acta 63 (1999) 4119–4138.

[30] A.J. Pietruszka, K.H. Rubin, M.O. Garcia, ^{226}Ra–^{230}Th–^{238}U disequilibria of historical Kilauea lavas (1790–1982) and the dynamics of mantle melting within the Hawaiian plume, Earth Planet. Sci. Lett. 186 (2001) 15–31.

[31] K.W.W. Sims, S.J. Goldstein, J. Blichert-Toft, M.R. Perfit, P. Kelemen, D.J. Fornari, P. Michael, S.R. Hart, D.J. DePaolo, G. Layne, L. Ball, M. Jull, J. Bender, Chemical and isotopic constraints on the generation and transport of magma beneath the East Pacific Rise, Geochim. Cosmochim. Acta 66 (2002) 3481–3504.

[32] M. Jull, P. Kelemen, K.W.W. Sims, Consequences of diffuse and channelled porous melt migration on uranium series disequilibria, Geochim. Cosmochim. Acta 66 (2002) 4133–4148.

[33] C. Lundstrom, Models of U-series disequilibria generation in MORB: the effects of two scales of melt porosity, Phys. Earth Planet. Inter. 121 (2001) 189–204.

[34] A.E. Saal, J.A. Van Orman, The ^{226}Ra enrichment in oceanic basalts: evidence for diffusive interaction within the crust–mantle transition zone, Geochem. Geophys. Geosys. 5 (2004) Q02008, doi:10.1029/2003GC000620 (pp000617).

[35] M. Spiegelman, UserCalc: a web-based uranium series calculator for magma migration problems, Geochem. Geophys. Geosys. 1 (2000) 11.

[36] K.W.W. Sims, D.J. Depaolo, M.T. Murrell, W.S. Baldridge, S.J. Goldstein, D.A. Clague, Mechanisms of magma generation beneath Hawaii and Midocean ridges—uranium/thorium and samarium/neodymium isotopic evidence, Science 267 (1995) 508–512.

[37] C. Claude-Ivanaj, B. Bourdon, C.J. Allegre, Ra–Th–Sr isotope systematics in Grande Comore Island: a case study of plume–lithosphere interaction, Earth Planet. Sci. Lett. 164 (1998) 99–117.

[38] N. Vigier, B. Bourdon, J.L. Joron, C.J. Allègre, U-decay series and trace element systematics in the 1978 eruption of Ardoukoba, Asal rift: timescale of magma crystallization, Earth Planet. Sci. Lett. 174 (1999) 81–97.

[39] B. Bourdon, S.P. Turner, N.M. Ribe, Partial melting and upwelling rates beneath the Azores from a U-series isotope perspective, Earth Planet. Sci. Lett. 239 (2005) 42–56.

[40] E.H. Hauri, J.A. Whitehead, S.R. Hart, Fluid dynamic and geochemical aspects of entrainment in mantle plumes, J. Geophys. Res. 99 (1994) 24275–24300.

[41] N.M. Ribe, U.R. Christensen, The dynamical origin of Hawaiian volcanism, Earth Planet. Sci. Lett. 171 (1999) 517–531.

[42] S. Watson, D. McKenzie, Melt generation by plumes: a study of Hawaiian volcanism, J. Petrol. 32 (1991) 501–537.

[43] T.F. Kokfelt, K. Hoernle, F. Hauff, Upwelling and melting of the Iceland plume from radial variation of ^{238}U–^{230}Th disequilibria in postglacial volcanic rocks, Earth Planet. Sci. Lett. 216 (2003) 1–20.

[44] C. Claude-Ivanaj, J.-L. Joron, C.J. Allegre, ^{238}U–^{230}Th–^{226}Ra fractionation in historical lavas from the Azores: long-lived source heterogeneity vs. metasomatism fingerprints, Chem. Geol. 176 (2001) 295–310.

[45] J.D. Blundy, B.J. Wood, Mineral-melt partitioning of Uranium, Thorium and their daughters, in: B. Bourdon, C. Lundstrom, G. Henderson, S.P. Turner (Eds.), U-Series Geochemistry, vol. 52, Mineralogical Society of America, 2003, pp. 59–118.

[46] C.C. Lundstrom, D.E. Sampson, M.R. Perfit, J. Gill, Q. Williams, Insights into mid-ocean ridge basalt petrogenesis: U-series disequilibria from the Siqueiros Transform, Lamont Seamounts, and East Pacific Rise, J. Geophys. Res. 104 (1999) 13035–13048.

[47] M.E. Sturm, S.J. Goldstein, E.M. Klein, J.A. Karson, M.T. Murell, Uranium-series age constraints on lavas from the axial valley of the Mid-Atlantic Ridge, MARK area, Earth Planet. Sci. Lett. 181 (2000) 61–70.

[48] F.J. Tepley, C. Lundstrom, K.W.W. Sims, R. Hekinian, U-series disequilibria in MORB from the Garrett transform and implications for mantle melting, Earth Planet. Sci. Lett. 223 (2004) 79–97.

[49] D. Landwehr, J. Blundy, E.M. Chamorro-Perez, E. Hill, B. Wood, U-series disequilibria generated by partial melting of spinel lherzolite, Earth Planet. Sci. Lett. 188 (2001) 329–348.

[50] V.J.M. Salters, J. Longhi, Trace element partitioning during the initial stages of melting beneath mid-ocean ridges, Earth Planet. Sci. Lett. 166 (1999) 15–30.

[51] P. McDade, J.D. Blundy, B.J. Wood, Trace element partitioning on the Tinaquillo Lherzolite solidus at 1.5GPa, Phys. Earth Planet. Inter. 39 (2003) 129–147.

[52] V.J.M. Salters, J.E. Longhi, M. Bizimis, Near mantle solidus trace element partitioning at pressures up to 3.4 GPa, Geochem. Geophys. Geosys. 3 (2002).

[53] W. van Westrenen, J. Blundy, B. Wood, Crystal-chemical controls on trace element partitioning between garnet and anhydrous silicate melt, Am. Min. 84 (1999) 838–847.

[54] W. van Westrenen, J.D. Blundy, B.J. Wood, High field strength element/rare earth element fractionation during partial melting in the presence of garnet: implications for identification of mantle heterogeneities, Geochem. Geophys. Geosys. 2 (2001) (Paper number 2000GC000133).

[55] M. Pertermann, M.M. Hirschmann, K. Hametner, D. Günther, M. W. Schmidt, Experimental determination of trace element partitioning between garnet and silica-rich liquid during anhydrous partial melting of MORB-like eclogite, Geochem. Geophys. Geosys. 5 (2004) Q05a01, doi:10.1029/2003GC000638 (pp.000623).

[56] S. Klemme, J.D. Blundy, B.J. Wood, Experimental constraints on major and trace element partitioning during partial melting of eclogite, Geochim. Cosmochim. Acta 66 (2002) 3109–3123.

[57] A. Stracke, V.J.M. Salters, K.W.W. Sims, Assessing the presence of garnet-pyroxenite in the mantle sources of basalts through combined hafniumneodymium-thorium isotope systematics, Geochem. Geophys. Geosys. 1 (1999) 000013 (Paper number 1999GC000013).

[58] M. Pertermann, M.M. Hirschmann, Trace element partitioning between vacancy-rich eclogitic clinopyroxene and silicate melt, Am. Min. 87 (2002) 1365–1376.

[59] B.J. Wood, J.D. Blundy, A.C. Robinson, The role of clinopyroxene in generating U-series disequilibrium during mantle melting, Geochim. Cosmochim. Acta 63 (1999) 1613–1620.

[60] B. Bourdon, A. Zindler, T. Elliott, C.H. Langmuir, Constraints on mantle melting at mid-ocean ridges from global ^{238}U–^{230}Th disequilibrium data, Nature 384 (1996) 231–235.

[61] H. Zou, A. Zindler, Y.L. Niu, Constraints on melt movement beneath the East Pacific Rise from ^{230}Th–^{238}U disequilibrium, Science 295 (2002) 107–110.

[62] K.H. Rubin, I. van der Zander, M.C. Smith, E.C. Bergmanis, Minimum speed limit for ocean ridge magmatism from ^{210}Pb–^{226}Ra–^{230}Th disequilibria, Nature 437 (2005) 534.

[63] S. Turner, S. Black, K. Berlo, ^{210}Pb–^{226}Ra and ^{228}Ra–^{232}Th systematics in young arc lavas: implications for magma degassing and ascent rates, Earth Planet. Sci. Lett. 227 (2004) 1–16.
[64] S. Turner, P. Evans, C. Hawkesworth, Ultrafast source-to-surface movement of melt at island arcs from ^{226}Ra–^{230}Th systematics, Science 292 (2001) 1363–1366.
[65] S.R. Hart, Equilibration during mantle melting—a fractal tree model, Proc. Natl. Acad. Sci. 90 (1993) 11914–11918.
[66] R.L. Nielsen, J. Crum, R. Bourgeois, K. Hascall, L.M. Forsythe, M.R. Fisk, D.M. Christie, Melt inclusions in high-An plagioclase from the Gorda ridge: an example of the local diversity of MORB parent magmas, Contrib. Mineral. Petrol. 122 (1995) 34–50.
[67] N. Shimizu, The geochemistry of olivine-hosted melt inclusions in a FAMOUS basalt ALV519-4-1, Phys. Earth Planet. Inter. 107 (1998) 183–201.
[68] A.V. Sobolev, N. Shimizu, Ultra-depleted primary melt included in an olivine from the Mid-Atlantic Ridge, Nature 363 (1993) 151–154.
[69] R. Sours-Page, K.T.M. Johnson, R.L. Nielsen, J.L. Karsten, Local and regional variation of MORB parent magmas: evidence from melt inclusions from the Endeavour segment of the Juan de Fuca ridge, Contrib. Mineral. Petrol. 134 (1999) 342–363.
[70] A.V. Sobolev, A.W. Hofmann, I.K. Nikogosian, Recycled oceanic crust observed in 'ghost plagioclase' within the source of Mauna Loa lavas, Nature 404 (2000) 986–990.
[71] A.E. Saal, S.R. Hart, N. Shimizu, E.H. Hauri, G.D. Layne, Pb isotopic variability in melt inclusions from oceanic island basalts, Polynesia, Science 282 (1998) 1481–1484.
[72] V.J.M. Salters, A. Stracke, Composition of the depleted mantle, Geochem. Geophys. Geosys. 5 (2004) 27, doi:10.1029/2003GC000597 (Q05004).
[73] B. Bourdon, J. Joron, C. Allegre, A method for ^{231}Pa analysis by thermal ionization mass spectrometry in silicate rocks, Chem. Geol. 157 (1999) 147–151.
[74] S.J. Goldstein, M.T. Murrell, D.R. Janecky, J.R. Delaney, D.A. Clague, Geochronology and petrogeneis of MORB form the Juan de Fuca and Gorda ridges by ^{238}U–^{230}Th disequilibrium, Earth Planet. Sci. Lett. 107 (1991) 25–41.
[75] C.C. Lundstrom, H.F. Shaw, F.J. Ryerson, Q. Williams, J. Gill, Crystal chemical control of clinopyroxene-melt partitioning in the Di–Ab–An system: implications for elemental fractionations in the depleted mantle, Geochim. Cosmochim. Acta 62 (1998) 2849–2862.
[76] D.W. Peate, C.J. Hawkesworth, P.W. vanCalsteren, R.N. Taylor, B.J. Murton, ^{238}U–^{230}Th constraints on mantle upwelling and plume–ridge interaction along the Reykjanes ridge, Earth Planet. Sci. Lett. 187 (2001) 259–272.
[77] S.J. Goldstein, M.T. Murrell, R.W. Williams, ^{231}Pa and ^{230}Th chronology of midocean ridge basalts, Earth Planet. Sci. Lett. 115 (1993) 151–159.
[78] D.A. Pickett, M.T. Murrell, Observations of ^{231}Pa/^{235}U disequilibrium in volcanic rocks, Earth Planet. Sci. Lett. 148 (1997) 259–271.
[79] C.C. Lundstrom, K. Hoernle, J.B. Gill, U-series disequilibria in volcanic rocks from the Canary Islands: plume versus lithospheric melting, Geochim. Cosmochim. Acta 67 (2003) 4153–4177.